NANO LETTERS
Letter
pubs.acs.org/NanoLett

Tunable Length and Optical Properties of $CsPbX_3$ (X = Cl, Br, I) Nanowires with a Few Unit Cells

Daniel Amgar, Avigail Stern, Dvir Rotem, Danny Porath, and Lioz Etgar*

The Institute of Chemistry, The Center for Nanoscience and Nanotechnology, The Casali Center for Applied Chemistry, The Hebrew University of Jerusalem, Jerusalem, Israel

Supporting Information

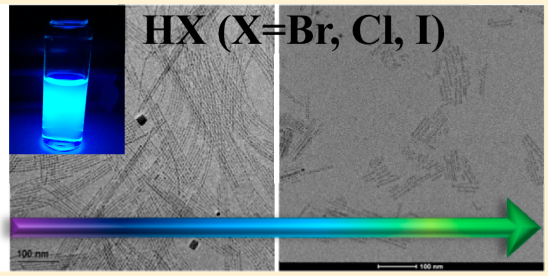

ABSTRACT: Perovskite nanostructures, both hybrid organo−metal and fully inorganic perovskites, have gained a lot of interest in the past few years for their intriguing optical properties in the visible region. We report on inorganic cesium lead bromide ($CsPbBr_3$) nanowires (NWs) having quantum confined dimensions corresponding to 5 unit cells. The addition of various hydrohalic acids (HX, X = Cl, Br, I) was found to highly affect the NW length, composition, and optical properties. Hydrochloric (HCl) and hydroiodic (HI) acids mixed in the reaction solution influence the crystal structure and optical properties and shorten the NWs, while the hydrobromic acid (HBr) addition results solely in shorter NWs, without any structural change. The addition of HX increases the acidity of the reaction solution, resulting in protonation of the oleylamine ligands from oleylamine into oleyl-ammonium cations that behave similarly to Cs^+ during crystallization. Therefore, the positions of the Cs^+ at the growing surface of the NWs are taken by the oleyl-ammonium cations, thus blocking further growth in the favored direction. The emission of the NWs is tunable between ∼423−505 nm and possesses a potential in the optoelectronic field. Moreover, electrical conductivity measurements of the NWs are discussed to give a new point of view regarding the conductivity of perovskite nanostructures.

KEYWORDS: *All-inorganic perovskite, transmission electron microscopy, nanowires, absorption, photoluminescence, electrical conductivity*

Perovskite materials aroused a great deal of interest among the solar and optoelectronic communities in recent years. In particular, bulk perovskite-based solar cells showed an impressive rise in photovoltaic performance in less than five years and reached an outstanding efficiency of 22.1%[1] to date. Holding such great promise, the perovskite research was extended to nanoforms of perovskite, both hybrid organo−metal and all-inorganic. Perovskite nanoparticles (NPs) are a family of new strongly emitting materials that can be optically tuned across the entire visible spectrum. In particular, all-inorganic perovskite, mostly known as $CsPbX_3$ (X = Cl, Br, I), appeared to be more stable because of the absence of an organic part in the crystal, thus being a good candidate for applications.

Previous publications vastly discussed the band gap tuning of $CsPbX_3$ NPs using compositional modifications and quantum size effects, and its characterization is still under investigation. Structural modifications, such as mixed halide systems (Br/I or Cl/Br) or postsynthetic halide exchange reactions, can tune the optical features by changing the halide content in the crystal.[2,3] Different halide contents lead to either a red or blue optical shift, according to the resulting band gap. Aside from modified composition, quantum size effects influence the band gap through quantum confinement. Various shapes of $CsPbX_3$ were studied, including nanocubes, nanosheets, nanoplates (NPLs), quantum dots, and nanowires (NWs).[4−8] Synthesis conditions, as well as the use of proper ligands in certain concentrations, have a large influence on the variety of $CsPbX_3$ NPs' morphologies, with the accompanied optical effects. Protesescue et al.[9] were the first to report on a synthesis of $CsPbX_3$ nanocubes with some preliminary optical and structural analyses. Very quickly, the field of $CsPbX_3$ perovskite NPs emerged extensively, and few groups started developing new methods to synthesize these particles. Zhang et al. had synthesized $CsPbX_3$ NWs by modifying the original synthesis. In this case, long NWs were formed in a longer growth time before quenching the reaction. Other groups reported on $CsPbX_3$ NPLs, where the injection temperature was lower than the one used for the original nanocubes synthesis.[10,11] The temperature appeared to dominate the shape of the NPs, and lower temperatures resulted in quasi 2D asymmetric morphologies. The relation between the reaction temperature and the product's shape was used by Akkerman et al.[11] who reported on a room temperature procedure to generate $CsPbBr_3$ NPLs. Further publications reported on nanosheets and NWs with even improved optical properties.[5−8] Apparently, the resulting NP shape and size are strongly dependent on the injection temperature and growth phase.

Received: October 19, 2016
Revised: December 22, 2016
Published: January 17, 2017

DOI: 10.1021/acs.nanolett.6b04381
Nano Lett. 2017, 17, 1007−1013

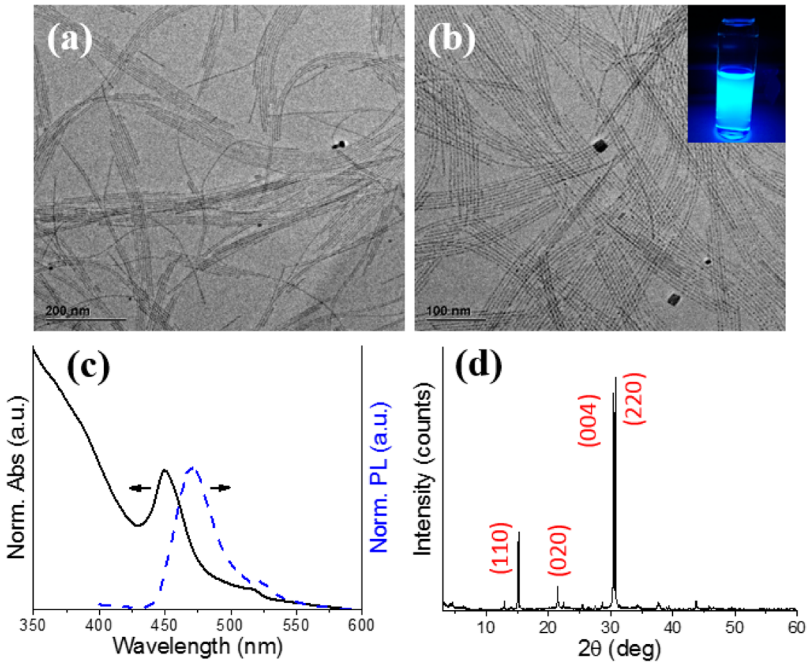

Figure 1. (a and b) Typical high-resolution transmission electron microscopy (HR-TEM) images of $CsPbBr_3$ NWs without the addition of any hydrohalic acid. The inset of b shows a photograph of the sample under UV light (λ = 365 nm). (c) Normalized absorption and PL spectra of $CsPbBr_3$ NWs without addition of any hydrohalic acid. The solid line refers to the absorption spectrum, and the dashed line refers to the PL spectrum. (d) X-ray diffraction (XRD) pattern of $CsPbBr_3$ NWs without the addition of any hydrohalic acid corresponds to a standard orthorhombic pattern of $CsPbBr_3$.

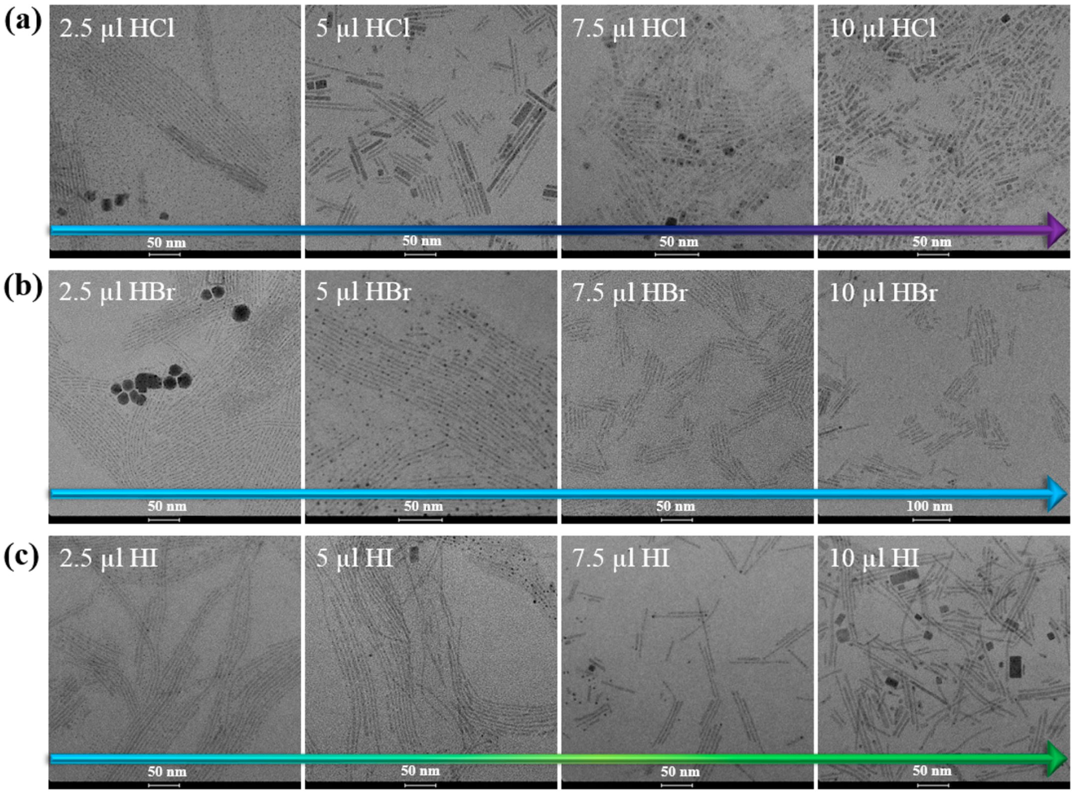

Figure 2. TEM images of the synthesized $CsPbX_3$ NWs. Panels a, b, and c present a series of samples with increasing amounts of HCl, HBr, and HI, respectively. The arrows indicate the direction of increasing the HX acid amount.

Here, we introduce $CsPbX_3$ NWs with dimensions of 5 unit cells exhibiting a significant quantum size effect in the absorption and emission spectra. We found that hydrohalic acids (HX, X= Cl, Br, I) influence the NW properties and demonstrated the effect for hydrochloric, hydrobromic, and hydroiodic acids (HCl, HBr, and HI, respectively). HX affects

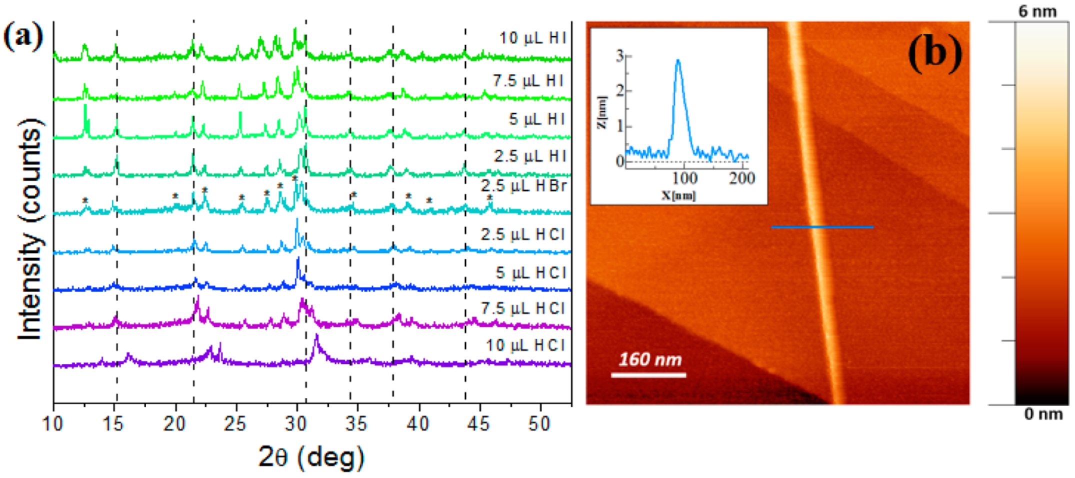

Figure 3. (a) X-ray diffraction (XRD) patterns of $CsPbBr_3$ NWs with different amounts of hydrohalic acids, including also the orthorhombic standard pattern of $CsPbBr_3$. The asterisk indicates nonrelated peaks of Cs_4PbBr_6. (b) Atomic force microscopy (AFM) scan of NWs deposited on freshly cleaved highly oriented pyrolytic graphite (HOPG). A NW of uniform 3 nm height is shown in the image. In accordance with TEM images, it is assumed to be a single NW. No lower NWs were imaged. Several NWs of similar height were observed in different scan areas as well as higher structures, assumed to be bundles. The inset represents a graph that corresponds to the scanned area.

the NWs in two ways: (i) Hydrohalic acids shorten the NWs. (ii) The halide in the hydrohalic acids participates in halide exchange reactions,[9] influencing their optical features. We varied the amounts of each acid in order to quantify the size change of the NWs upon increasing the HX amount. Structural, optical, and physical characterizations of the NWs were performed in order to establish an understanding of the mechanism of the NWs' formation and properties. In addition, electrical conductivity measurements of single NWs have been completed to give a novel view of the electrical properties of the reported NWs.

Results and Discussion. The synthesis of $CsPbX_3$ NWs was performed according to a previously published procedure by Akkerman et al.,[11] with slight changes. Hot cesium-oleate (Cs-oleate) and lead bromide ($PbBr_2$) precursor solutions were prepared for the source of the ions Cs^+, Pb^{2+}, and Br^-. Cs-oleate was synthesized under inert conditions using cesium carbonate (Cs_2CO_3), oleic acid (OA), and 1-octadecene (ODE). $PbBr_2$ precursor solution was prepared in dimethylformamide (DMF). The reaction was performed at room temperature by adding hot Cs-oleate to a vial that contained ODE, OA, oleylamine (OLA), and a variable amount of HX acid (0−10 μL). $PbBr_2$ precursor solution was added to the vial, and after 10 s acetone, which acted as an antisolvent, was swiftly added to the reaction mixture in order to quench the reaction, forming free-standing $CsPbBr_3$ NWs.

The first step was synthesizing NWs without any addition of acid. The product appeared as a dense net of micron-sized asymmetric nanostructures with width of ~3 nm, as shown in transmission electron microscope (TEM) images in Figure 1a,b. The obtained NWs were extremely narrow, while a width of ~3 nm corresponds to 5 unit cells.[11] A narrow size distribution of the width is shown in Figure S1, with an average width of ~3.3 nm. The inset of Figure 1b presents the product dispersed in hexane under UV light. The blue photoluminescence (PL) indicates a blue shift and enlargement of the band gap, relative to the reported cubic $CsPbBr_3$ NPs, which have a green PL, probably due to quantum confinement.[9] Figure 1c presents optical measurements of the synthesized NWs. The emission peak of previously reported cubic $CsPbBr_3$ was at ~519 nm,[7] while in this work the emission peak is located around 475 nm for $CsPbBr_3$ NWs without the addition of HX in the precursor solution. The significant blue shift in this case is attributed to quantum confinement of the NPs. According to the effective mass theory,[12] the calculated Bohr diameter of $CsPbBr_3$ is 7 nm,[9] which can explain the large blue shift. Furthermore, the synthesis took place at room temperature, thus enabled a better controlled growth of the NWs with a width of few unit cells only. X-ray diffraction (XRD) pattern of the synthesized $CsPbBr_3$ NWs, presented in Figure 1d, is in good agreement with the standard orthorhombic crystal structure of $CsPbBr_3$.[13] The low temperature of the synthesis enhanced crystallization in the orthorhombic phase, as previously reported.[7] Moreover, the asymmetric morphology of the NWs is well-supported by the narrow and sharp peak of the plane (004), which also has high intensity.

In order to investigate the effect of HX on the NWs, a series of increasing amounts of HX was prepared for each HX; 2.5 μL, 5 μL, 7.5 μL, and 10 μL. Variable amounts of the HX addition resulted in $CsPbX_3$ NWs with different lengths. Figure 2a,b,c shows TEM images of the synthesized NWs with different hydrohalic acids, HCl, HBr, and HI, respectively. In each series of NWs (Figure 2a,b,c) the arrows indicate an increase in the amount of HX. The nanostructures morphology is clearly that of NWs, and their shape was retained upon increasing the HX amount, while the length of the NWs was shortened with almost every increase. However, the width of the NWs remained the same, ~3 nm. There is a slight difference in the tendency of the shortening of the NWs' length among the three HX-based NWs that most probably arises from the acidity differences. A more acidic environment leads to an enhanced protonation of the oleylamine ligands into oleyl-ammonium cations, randomly occupying binding sites of Cs^+ ions in the lattice, and causing a shortening at a given amount of acid (discussed later in more detail). This interruption to the crystal growth creates a passivation layer and limits further crystallization. As shown in Figure 2, the shortening effect is different among the acids. As is well-known, the strength of an acid depends on the stability of its conjugated base; i.e., the equilibrium constant will determine the strength of an acid.

Hydrohalic acids are considered strong acids, while HCl is defined as a strong acid and both HBr and HI are defined as very strong acids. This is according to few factors including the free energy of bond breaking and hydration.[14,15] Accordingly, one would expect that HI and HBr will have a stronger shortening effect relative to HCl. This forecast does not necessarily fit the observations because the use of different concentrations of the acids and examining the shortening effect of each acid separately. The study of various HX aimed to show the tendency in which protons enhance shortening of the NWs and is consistent among different HX. Furthermore, additional species are observed in the TEM images, such as plates, small cubes, and quantum dots. It seems that in Figure 2a the shape of the NWs changes upon adding more HCl. This can be explained by the acidity considerations discussed above and disruption of the lattice. It is possible that the extremely acidic environment affects also the other facets of the NWs and thus yields a distortion of NW shapes toward a more plate-like shape. The random nature of the passivating effect by oleylammonium cations is prominent in Figure 2. Each fraction of HX results with a large distribution of the NWs length, which was hard to estimate. Addition of increasing amounts of HBr seems to result in shorter NWs, as presented in Figure 2b (HBr-based $CsPbBr_3$ NWs), but less distorted shapes and less side products were observed, relative to Figure 2a (HCl-based NWs). It may be related to halide exchange processes that occur spontaneously. For HBr-based NWs, halide exchange process caused a replacement between two identical ions (Br^-), one originated from HBr and the other from the original NWs ($CsPbBr_3$). This kind of ion exchange process is less destructive to the crystal structure than the ones with HCl and HI. Apparently, in Figure 2c, the influence of HI is less dramatic, while the difference between every two consequent fractions (for example, the fractions of 7.5 and 10 μL) is milder. The black dots that appear in some of the TEM images were already reported in previous work[10] and were recognized as lead particles that formed after an exposure to the electron beam.

Figure 3a depicts the structural analysis of the synthesized NWs through XRD and emphasizes the effect of different HX amounts on the crystal structure. The addition of HCl and HI led to partial ion exchange processes, depending on the amount of acid added, while HBr showed no significant change in the crystal structure because it is an exchange of the same halide (see Figure S2). The XRD patterns show a small right shift, to higher angles, for HCl-based NWs, and the opposite trend is seen for HI-based NWs, relating to the peaks of orthorhombic $CsPbBr_3$ crystal structure. The shift to higher angles can be explained by the halide size and the space it occupies in the lattice. Cl^- is smaller than Br^-; thus the substitution of some of the Br^- anions with Cl^- anions can lead to a contraction of the lattice. Similarly, the substitution of Br^- anions with I^- anions can lead to an expansion of the lattice.[16] Another observation from the structural analysis in Figure 3a is the coexistence of a nonperovskite Cs_4PbBr_6 phase along with the $CsPbBr_3$ phase. An undesired existence of Cs_4PbBr_6, previously reported, derives most probably from an inevitable unsuitable melting growth process.[17] The asterisks in Figure 3a indicate peaks that are attributed to the parasitic Cs_4PbBr_6 phase and not to the orthorhombic crystal structure of $CsPbX_3$ perovskite. In addition, the reduction of this phase for HCl-based NWs and an increase for HI-based NWs were observed, possibly caused by a mismatch or a match, respectively, between the exchanged crystal and the Cs_4PbBr_6 phase. Figure 3b presents an atomic force microscopy (AFM) measurement of the NWs. Topographic AFM scanning showed elongated structures of micrometers length, the lowest of which had a rather uniform height of ~3 nm (see the inset in Figure 3b). Probably, the 3 nm high structures are single NWs, in accordance with dimensions seen in TEM imaging. Higher structures may be bundles of several NWs or single NWs wrapped in organic substance. More areas were scanned, and the detected NWs can be viewed in the Supporting Information (SI) section (Figure S3).

Figure 4a presents optical measurements of all of the synthesized NWs. The significant blue shift in this case is related to quantum confinement of the NWs, as mentioned above. The existence of two peaks in some of the measurements indicates two populations of nanostructures; one is the NWs, and the other is red-shifted and belongs to another population, such as larger cubic-shaped $CsPbBr_3$. The perovskite crystal has an ionic nature,[9] and therefore, a fast ion exchange can easily occur among halides in solution. In Figure 4a, an addition of either HCl or HI causes a blue or a red shift, respectively, in the absorption and emission spectra. As the ion exchange process proceeds, more ions are exchanged within the crystal, and the exciton peak shifts to higher or lower wavelengths, according to the exchanged lattice. As for the increasing amount of HBr, the optical properties remained almost the same, as presented in Figure S4. Figures 4b,c,d show photographs of all of the synthesized NWs, visualizing the PL of the NWs as well as the optical tuning caused by the unavoidable halide exchange processes in solution. For HI-based NWs, the emission red shift from blue to green (Figure 4b) indicates that some bromide ions were exchanged with iodide ions, and the emission blue shift from light blue to dark blue (Figure 4d) indicates that some bromide ions were exchanged with chloride ions.

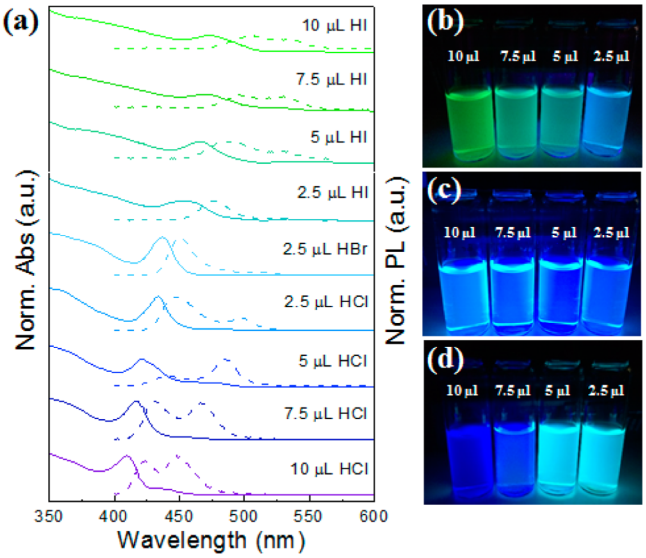

Figure 4. (a) Normalized absorption and normalized photoluminescence (PL) spectra of the various sample of $CsPbX_3$ NWs. The solid lines refer to absorption spectra, and dashed lines refer to PL spectra. Panels b, c, and d present photographs of the synthesized NWs with addition of HI, HBr, and HCl acids, respectively, under UV light (λ = 365 nm).

Figure 5 presents a schematic illustration that describes the effect of HX on the NWs' length in more detail. In the scheme,

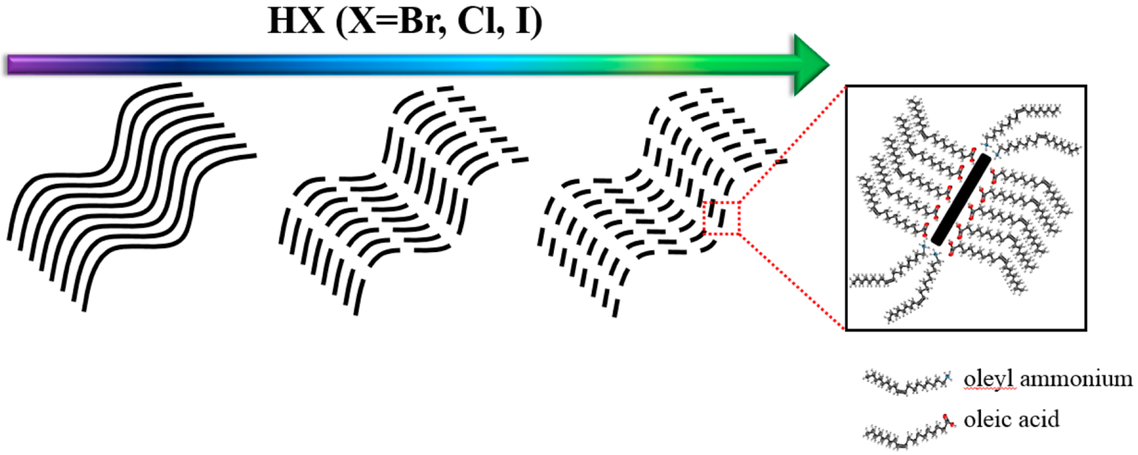

Figure 5. Schematic illustration of the passivation effect by hydrohalic acids on the length of $CsPbX_3$ NWs.

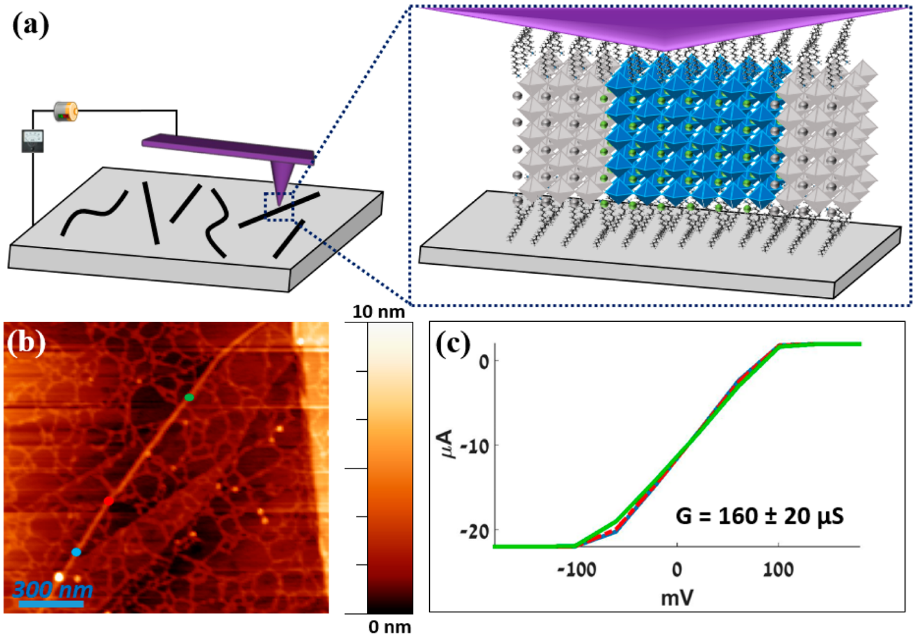

Figure 6. (a) Schematic illustration of conductive AFM (cAFM) setup. (b) cAFM scanning area with the measured NW. (c) *IV* curves that describe the electrical conductivity in three different points on a single NW, which correspond to the colored points shown in b.

the first stage represents NWs that were synthesized without adding acid to the reaction mixture. The addition of HX increases the acidity of the reaction solution, resulting in the protonation of the oleylamine ligands from oleylamine into oleyl-ammonium cations that behave similarly to Cs^+, as previously suggested by other groups as well.[18,19] Most likely, the protonated oleylamine molecules imitate the Cs^+ during the crystallization of $CsPbX_3$ perovskite and compete with the Cs^+ cations on the active surface of the growing NWs. The binding of oleyl-ammonium ligands creates a passivation layer on the growing surface of the NWs. In a typical synthesis, Cs^+, Pb^{2+}, X^-, and oleyl-ammonium cation immediately crystallize into NW structures, after an addition of a polar solvent (acetone was used here) that induces precipitation of the NWs. In the resulting NWs, some of the positions of the Cs^+ at the growing surface are taken by the oleyl-ammonium cations, thus blocking further growth in the favored direction by the long oleic chain. The oleyl-ammonium ligands create a steric interference and probably cannot function as intrinsic organic cations within the perovskite crystal. This competition between Cs^+ and oleyl-ammonium cations yields in random shorter NWs, while the larger amount of HX raises this length-reducing passivation effect.

In addition to the optical measurements, the electrical conductivity of the NWs was studied. The electrical conductivity of these new perovskite nanowires is of utmost importance for their performance in various applications. Figure 6 shows transverse electrical characterization of the NWs. Figure 6a presents a scheme of the conductive AFM (cAFM) setup for measuring across NWs with 5 unit cells. Figure 6b,c presents cAFM measurements across the NWs that gave linear *I*−*V* curves (more details in Supporting Information). The average conductance extracted from 15 such curves measured on the two nanowires with the highest conductivity was 160 ± 20 μS. This conductivity is a lower limit for the actual conductivity across the NWs due to the contribution of additional resistances in the measured setup, such as contamination and/or tip-nanowire contact resistance.

Experimental Section. *Chemicals.* Cesium carbonate (Cs_2CO_3, 99.9%, Sigma-Aldrich), lead(II) bromide ($PbBr_2$,

≥98%, Sigma-Aldrich), oleic acid (OA, 90%, Sigma-Aldrich), oleylamine (OLAM, 70%, Sigma-Aldrich), 1-octadecene (ODE, 90%, Sigma-Aldrich), hydrochloric acid (HCl, 37%, Sigma-Aldrich), hydrobromic acid (HBr, ≥99.99%, Sigma-Aldrich), hydroiodic acid (HI, 99.99%, Sigma-Aldrich), dimethylformamide (DMF, 99.8%, Holland Moran), acetone (not pure, Gadot), and hexane (not pure, Gadot) were purchased and used as received, without any further purification.

Preparation of Cs-Oleate. Cs-oleate precursor was prepared according to previous published procedure by Protesescue et al.[9] 0.4 g of Cs_2CO_3 were mixed with 1.25 mL of oleic acid (OA) and 15 mL of 1-octadecene (ODE) in a 100 mL 3-neck flask. The solution was degassed for 1 h under vacuum at 120 °C and then heated to 150 °C under Ar flow.

Synthesis of $CsPbBr_3$ NWs. The NWs were synthesized according to Akkerman et al.[11] with slight changes. A solution of 1.25 mL of ODE, 0.125 mL of oleic acid, 0.125 mL of oleylamine (OLA), and a variable amount of hydrohalic acid (HBr/HCl/HI, 0−10 μL) were loaded in a glass vial. 0.1 mL of Cs-oleate (the syringe was heated before injection) were added to the reaction vial. 0.2 mL of $PbBr_2$ precursor solution (0.4 M, 0.735 g of $PbBr_2$ in 5 mL of DMF, heated for 1 h at 80 °C until full dissolution) was added into the reaction vial. After 10 s, 5 mL of acetone were swiftly added to trigger the crystallization of the $CsPbBr_3$ NWs. The solution turned turbid white and then gradually changed its color to green. The NWs were precipitated by centrifugation at 3000 rpm for 5 min. The purified product was redispersed in hexane. Additional purification steps ruined the NWs.

The synthesis took place at room temperature.

Transmission Electron Microscopy (TEM). Typical TEM images were taken using both Tecnai F20 G2 (FEI Company, U.S.A.) and Tecnai T12 G2 Spirit (FEI Company, U.S.A.). Sample preparation was performed as follows: 3.5 μL of the NW dispersion was dripped on a copper grid coated with amorphous carbon film; then the solvent was evaporated using a vacuum chamber.

X-ray Diffraction (XRD). Powder X-ray diffraction measurements were performed in grazing incidence X-ray diffraction (GIXRD) mode on the D8 Advance Diffractometer (Bruker AXS, Karlsruhe, Germany) with a goniometer radius of 217.5 mm, a secondary graphite monochromator, 2° Soller slits, and a 0.2 mm receiving slit. XRD patterns within the range 3−60° 2θ were recorded at room temperature using CuKa radiation (l 1/4 1.5418°A) with the following measurement conditions: tube voltage of 40 kV, tube current of 40 mA, step-scan mode with a step size of 0.02° 2θ, and counting time of 1−3 s per step. The value of the grazing incidence angle was 2.5°.

Absorption and Photoluminescence Measurements. Absorption spectra were recorded using Jasco V-670 spectrophotometer. Photoluminescence (PL) measurements were performed using L-shaped spectrofluoremeter (Edinburgh Instruments FL920). The samples were excited at 350 nm. The emission was collected at 90° at the range of 400−600 nm.

Atomic Force Microscopy (AFM). Topography and conductivity measurements were performed on the NWs after their deposition on HOPG substrate. A drop of solution was deposited onto freshly cleaved 1 × 1 cm^2 HOPG, then dried in a pumped hood, rinsed with acetone and allowed to dry again. AFM topography images were obtained with Nanotec Electronica (Madrid, Spain) AFM system in dynamic (tapping) mode using 100 μm long silicon nitride cantilevers (Olympus, OMCL-RC800PSA-W) with resonance frequency of 70 kHz and 15 nm nominal radius. Conductive AFM measurements were performed with Smart-AIST conductive AFM system using Cr/Pt coated ~200 μm long silicon cantilevers (Budget Sensors, Multi75E-G) with resonance frequency 75 kHz. After scanning the sample in AC (tapping) mode, measurements were performed at chosen locations. Measurements were performed by sweeping the voltage from −2 V to +2 V and measuring current after contacting the sample with a ~50 nN normal force. The images were analyzed and visualized using a Nanotec Electronica S.L (Madrid) WSxM imaging software.[20]

Conclusions. This report describes the synthesis of $CsPbBr_3$ NWs in ambient conditions. The synthesized NWs show a narrow size distribution of ~3 nm having two quantum confined dimensions proved by TEM and AFM measurements. Hydrohalic acids influence the NWs in two aspects: (i) shortening of the NWs with increasing the amount of acid added, and (ii) alteration of compositional structure and optical properties, induced by halide exchange reactions in the case of nonidentical ions of the acid and the crystal. For example, such a reaction can be induced by addition of HCl to the precursor solution that contained Br^- ions. We concluded that the acidity of the hydrohalic acids is a decisive factor for the NWs' properties, as well as the halide content in the acid. In general, all of the hydrohalic acids are considered strong acids that can promote protonation of amines. We deduced that the protonation of the amine ligands was the key to the shortening of micrometer-long NWs. In addition, this work includes some new insights regarding the electrical conductivity properties of the reported NWs through 5 unit cells. cAFM measurements show a lower limit conductivity of 160 ± 20 μS for a single NW.

The asymmetric nature of the reported NWs can pave the way to an oriented growth of another semiconductor via an epitaxial growth of two or more semiconducting materials. This can open new possibilities to produce systems for energy transport, taking into consideration the optical and physical features of such nanocomposites. In addition, the $CsPbX_3$ NWs can be applied as emitting materials in light-emitting devices.

■ ASSOCIATED CONTENT

Ⓢ Supporting Information

The Supporting Information is available free of charge on the ACS Publications website at DOI: 10.1021/acs.nanolett.6b04381.

Size distribution of the NW width, XRD spectra of Br-based NWs with various amounts of HBr, AFM scans of different NWs and absorption, emission spectra of Br-based NWs with various amounts of HBr, and current−voltage measurements using conductive AFM on several NWs and on the nearby HOPG substrate (PDF)

■ AUTHOR INFORMATION

Corresponding Author

*E-mail: lioz.etgar@mail.huji.ac.il.

ORCID

Lioz Etgar: 0000-0001-6158-8520

Notes

The authors declare no competing financial interest.

ACKNOWLEDGMENTS

We would like to thank the China-Israel program and the Ministry of Energy for their support. D.P. is supported by the Israel Science Foundation (ISF grant 1589/14) and by the Minerva Centre for biohybrid complex systems. D.P. thanks the Etta and Paul Schankerman Chair of Molecular Biomedicine.

REFERENCES

(1) http://www.nrel.gov/ncpv/images/efficiency_chart.jpg; Sept 30, 2016.
(2) Nedelcu, G.; Protesescue, L.; Yakunin, S.; Bodnarchuk, M. I.; Grotevent, M. J.; Kovalenko, M. V. *Nano Lett.* **2015**, *15*, 5635.
(3) Hoffman, J. B.; Schleper, A. L.; Kamat, P. V. *J. Am. Chem. Soc.* **2016**, *138*, 8603.
(4) Sun, S.; Yuan, D.; Xu, Y.; Wang, A.; Deng, Z. *ACS Nano* **2016**, *10*, 3648.
(5) Shamsi, J. S.; Dang, Z.; Bianchini, P.; Canale, C.; Stasio, F. D.; Brescia, R.; Prato, M.; Manna, L. *J. Am. Chem. Soc.* **2016**, *138*, 7240.
(6) Eaton, S. W.; Lai, M.; Gibson, N. A.; Wong, A. B.; Dou, L.; Ma, J.; Wang, L. W.; Leone, S. R.; Yang, P. *Proc. Natl. Acad. Sci. U. S. A.* **2016**, *113* (8), 1993.
(7) Zhang, D.; Eaton, S. W.; Yu, Y.; Dou, L.; Yang, P. *J. Am. Chem. Soc.* **2015**, *137*, 9230.
(8) Zhang, D.; Yang, Y.; Bekenstein, Y.; Yu, Y.; Gibson, N. A.; Wong, A. B.; Eaton, S. W.; Kornienko, N.; Kong, Q.; Lai, M.; Alivisatos, A. P.; Leone, S. R.; Yang, P. *J. Am. Chem. Soc.* **2016**, *138*, 7236.
(9) Protesescue, L.; Yakunin, S.; Bodnarchuk, M. I.; Krieg, F.; Caputo, R.; Hendon, C. H.; Yang, R. X.; Walsh, A.; Kovalenko, M. V. *Nano Lett.* **2015**, *15*, 3692.
(10) Bekenstein, Y.; Koscher, B. A.; Eaton, S. W.; Yang, P. Y.; Alivisatos, A. P. *J. Am. Chem. Soc.* **2015**, *137*, 16008.
(11) Akkerman, Q. A.; Motti, S. G.; Kandada, A. R. S.; Mosconi, E.; D'Innocenzo, V.; Bertoni, G.; Marras, S.; Kamino, B. A.; Miranda, L.; De Angelis, F.; Petrozza, A.; Prato, M.; Manna, L. *J. Am. Chem. Soc.* **2016**, *138*, 1010.
(12) Yu, P. Y.; Cardona, M. *Fundamentals of semiconductors*; Springer, 1996.
(13) Cottingham, P.; Brutchey, R. L. *Chem. Commun.* **2016**, *52*, 5246.
(14) Myers, R. T. *J. Chem. Educ.* **1976**, *53*, 17.
(15) Schmid, R.; Miah, A. M. *J. Chem. Educ.* **2001**, *78*, 116.
(16) Zhang, D.; Yang, Y.; Bekenstein, Y.; Yu, Y.; Gibson, N. A.; Wong, A. B.; Eaton, S. W.; Kornienko, N.; Kong, Q.; Lai, M.; Alivisatos, A. P.; Leone, S. R.; Yang, P. *J. Am. Chem. Soc.* **2016**, *138*, 7236.
(17) Nikl, M.; Mihokova, E.; Nitsch, K.; Somma, F.; Giampaolo, C.; Pazzi, G. P.; Fabeni, P.; Zazubovich, S. *Chem. Phys. Lett.* **1999**, *306*, 280.
(18) Sichert, J. A.; Tong, Y.; Mutz, N.; Vollmer, M.; Fischer, S.; Milowska, K. Z.; Cortadella, R. G.; Nickel, B.; Cardenas-Daw, C.; Stolarczyk, J. K.; Urban, A. S.; Feldmann, J. *Nano Lett.* **2015**, *15*, 6521.
(19) Yuan, Z.; Shu, Y.; Tian, Y.; Xin, Y.; Ma, B. *Chem. Commun.* **2015**, *51*, 16385.
(20) Horcas, I.; Fernandez, R.; Gomez-Rodriguez, J. M.; Colchero, J.; Gomez-Herrero, J.; Baro, A. M. *Rev. Sci. Instrum.* **2007**, *78*, 013705.